ELSEVIER

Catalysis Today 70 (2001) 331–340

CATALYSIS TODAY

www.elsevier.com/locate/cattod

Front dynamics in catalytic surface reactions

Ehud Meron [a,b,*], Markus Bär [c], Aric Hagberg [d], Uwe Thiele [c,e]

[a] *Department of Solar Energy and Environmental Physics, BIDR, Ben-Gurion University, Sede Boker Campus 84990, Israel*
[b] *Department of Physics, Ben-Gurion University, Beer Sheva 84105, Israel*
[c] *Max-Planck-Institut für Physik komplexer Systeme, Nöthnitzer Street 38, 01187 Dresden, Germany*
[d] *Los Alamos National Laboratory, Center for Nonlinear Studies and T-7, Theoretical Division, Los Alamos, NM 87545, USA*
[e] *Instituto Pluridisciplinar, Universidad Complutense Madrid, Paseo Juan XXIII 1, E-28040 Madrid, Spain*

Abstract

A variety of pattern formation phenomena in catalytic surface reactions can be attributed to the dynamics of interfaces, or fronts, separating distinct uniform states. The states may represent surface coverages by different adsorbates or in the case of forced oscillations, different phases of oscillation. The dynamics of fronts are strongly affected by front instabilities and by diffusion anisotropy. We identify two new pattern formation mechanisms associated with different front behaviors in orthogonal directions: an ordering process by which stationary labyrinths in an isotropic system evolve into ordered stationary stripes, and confinement of isotropic spatiotemporal chaos to one space dimension, a state we term *stratified chaos*.

PACS: 82.20.Mj; 05.45.−a

Keywords: Catalytic reaction; Anisotropy; Front instabilities; Stratified chaos

1. Introduction

Heterogeneous catalytic reactions, involving adsorption and desorption of molecular species on crystal surfaces, provide a wealth of nonlinear dynamics and pattern formation phenomena on micrometer to millimeter scales. These phenomena include spontaneous oscillations and entrainment in forced oscillations [1], front [2,3] and pulse [4] dynamics and spiral waves [5,6]. The micrometer-scale dynamics are often associated with spatiotemporal processes at a smaller (nanometer) scale such as surface phase transitions induced by adsorption of molecular species [1]. The wide range of length scales in catalytic surface reactions makes them excellent subjects for investigating the relations between dynamics at micro-scales and nano-scales, and for studying the potential control of nanostructures by manipulating patterns at the micro-scale.

Two theoretical approaches are being used to bridge over the different length scales: a top-down approach involving phenomenological macroscopic models for the reaction schemes [1], and a bottom-up approach using Monte-Carlo simulations [7,8] and microscopic models [9]. This paper belongs to the former category. We consider a class of pattern formation mechanisms at the micrometer to millimeter scales associated with single fronts which are the smallest structures at these scales. The mechanisms pertain to instabilities of the

* Corresponding author. Present address: Department of Solar Energy and Environmental Physics, BIDR, Ben-Gurion University, Sede Boker Campus 84990, Israel. Tel.: +972-7659-6926; fax: +972-7659-6921.
E-mail addresses: ehud@bgumail.bgu.ac.il (E. Meron), baer@mpipks-dresden.mpg.de (M. Bär), aric@lanl.gov (A. Hagberg), thiele@mpipks-dresden.mpg.de (U. Thiele).

0920-5861/01/$ – see front matter
PII: S0920-5861(01)00341-8

front structures themselves [10–12]. Single front structures may form in catalytic reactions with bistability of two stationary uniform states [3,13,14], or in oscillatory reactions subjected to time-periodic modulation of a control parameter. Periodic forcing at twice the unforced reaction frequency fixes the phase of oscillation at two possible values differing by π. Phase fronts that shift the oscillation phase by π may form between these two phase states [15,16].

An example of a catalytic surface reaction which has both oscillations and bistability of stationary states is the CO oxidation on Pt(1 1 0), Pt(1 0 0), and Pt(2 1 0) surfaces [1]. Oscillations in this reaction consist of surface phase transitions between a CO covered 1×1 phase with a high oxygen sticking coefficient and a CO depleted reconstructed phase with a low oxygen sticking coefficient. Periodic forcing of the reaction on Pt(1 1 0) has been studied by modulating the partial pressure of oxygen [17].

In a different parameter range bistability of stationary states, a CO covered surface and an oxygen covered surface, has been observed. A simple bistability with a unique front solution was theoretically predicted [18] and experimentally verified [19] in the CO oxidation on Pt(1 1 1) where no reconstruction occurs. A significant observation made in CO oxidation experiments on Pt(1 0 0) and Pt(1 1 0) is the coexistence of two stable fronts, pertaining to CO covered state invading an oxygen covered state (a "CO front"), and an oxygen covered state invading a CO covered state (an "oxygen front"). This coexistence of fronts, referred to as "dynamic bistability" [14,20], has been attributed to a front bifurcation [14]. Further studies revealed the same phenomenon also in the $NO + H_2$ reaction on Rh(1 1 0) [21]. Presumably, it is also of relevance for the rich spatiotemporal dynamics discovered in the CO oxidation on Pt(2 1 0) [22]. In a symmetric setting, this is a pitchfork bifurcation that renders a stationary front unstable and produces a pair of counter-propagating stable fronts. Front bifurcations of this type have been found both in nonoscillatory bistable systems [10,23,24] and in periodically forced oscillatory systems [15]. They are referred to as "nonequilibrium Ising–Bloch (NIB) bifurcations".

In this paper, we study pattern formation mechanisms resulting from the coupling of the NIB bifurcation to the crystal surface anisotropy [25,26]. Anisotropy has a dramatic impact on chemical waves on catalytic surfaces. Square-shaped waves have been seen in the reaction of NO and H_2 on Rh(1 1 0) [21,27,28], while the reaction of O_2 and H_2 on Rh(1 1 1) displays triangular patterns [29]. To simplify the analysis, we use a FitzHugh-Nagumo (FHN) model with diffusion anisotropy. More realistic models which also have a NIB bifurcation are expected to exhibit similar behaviors. In Section 2, we present the anisotropic FHN model and describe two types of front instabilities: the NIB bifurcation and transverse (or morphological) instability. We also present the normal form equation for periodically forced oscillations and discuss the NIB bifurcation in that context. In Section 3, we study the effects of diffusion anisotropy on the velocity of curved fronts by deriving the angular dependence of velocity–curvature relations. These relations are used in Section 4 to study the effects of anisotropy on the two types of front instabilities. These effects suggest new mechanisms of pattern formation which we describe in Section 5. We conclude with a discussion in Section 6.

2. The model

Phenomenological models with parameters deduced from experimental data have been developed for several surface reactions including CO oxidation on platinum surfaces [30]. The rate equations involve adsorption, desorption, dissociation, and reaction terms. The spatial coupling is provided by surface diffusion of some adsorbed species with anisotropy of the diffusion being either intrinsic or induced by adsorbate coverages. Many qualitative features of models of this kind are captured by FHN models describing oscillatory or bistable media [10]. The specific model we choose to study is

$$\frac{\partial u}{\partial t} = \epsilon^{-1}(u - u^3 - v) + \delta^{-1}\nabla^2 u + \frac{\partial}{\partial y}\left[d\delta^{-1}\frac{\partial u}{\partial y}\right],$$
$$\frac{\partial v}{\partial t} = u - a_1 v - a_0 + \nabla^2 v, \qquad (1)$$

where u is the activator and v the inhibitor. The parameter a_0 can be regarded as a bias parameter which breaks the odd symmetry of the system, $(u, v) \to (-u, -v)$ at $a_0 = 0$. The parameter a_1 can be chosen so that Eqs. (1) represent an oscillatory medium arising from a Hopf bifurcation of the $(u, v) = (0, 0)$

state to uniform oscillations ($a_1 < 1$), or a bistable medium with two stationary and uniform stable states, an "up" state, (u_+, v_+), and a "down" state, (u_-, v_-) ($a_1 > 1$). For the symmetric system ($a_0 = 0$), the Hopf bifurcation occurs as ϵ is decreased past $\epsilon_c = a_1^{-1}$. The Hopf frequency is $\omega_0 = \sqrt{a_1^{-1} - 1}$. The parameter d introduces diffusion anisotropy.

We now review a few results for isotropic systems ($d = 0$). Consider first bistable systems ($a_1 > 1$) [10–12], where the coexistence of up and down states allows for fronts solutions connecting the two states in space. In the symmetric case ($a_0 = 0$), a stationary front solution exists. This solution loses stability to a pair of counter-propagating fronts in a pitchfork bifurcation as ϵ or δ is decreased below some critical values. For $\epsilon/\delta \ll 1$, the bifurcation point is given by $\eta = \eta_c$, where $\eta = \sqrt{\epsilon\delta}$, $\eta_c = \frac{3}{2}\sqrt{2}q^3$ and $q^2 = a_1 + \frac{1}{2}$. This is the NIB bifurcation. The stationary front is often called an "Ising front", while the two counter-propagating fronts are called "Bloch fronts". The corresponding bifurcation diagram is shown in Fig. 1(a). Breaking the odd symmetry by setting $a_0 \neq 0$ unfolds the pitchfork bifurcation into a saddle-node bifurcation as shown in Fig. 1(b).

Any of the front solutions may be unstable to transverse perturbations where modulations of a linear front begin to grow. For the symmetric system ($a_0 = 0$) and for $\epsilon/\delta \ll 1$, the thresholds for these instabilities are given by $\delta = \delta_I(\epsilon) = \epsilon/\eta_c^2$ and $\delta = \delta_B(\epsilon) = \eta_c/\sqrt{\epsilon}$ for Ising and Bloch fronts, respectively. A diagram in the (ϵ, δ) plane, displaying the NIB bifurcation boundary, $\delta = \delta_F(\epsilon)$, and the transverse instability boundaries, $\delta = \delta_I(\epsilon)$ and $\delta = \delta_B(\epsilon)$, is shown in Fig. 2.

Consider now the oscillatory case ($a_1 < 1$) [15,16,31,32] with the system periodically forced at a frequency $\omega_f \approx 2\omega_0$. Close to the Hopf bifurcation of the $(u, v) = (0, 0)$ state any of the state variables can be expanded as power series in $\mu = \sqrt{(\epsilon_c - \epsilon)/\epsilon_c}$: $u = \mu u_1 + \mu^2 u_2 + \cdots$, where $u_1 = A\exp(i\omega_f t/2) + \text{c.c.}$ (and similarly for v). An equation for the amplitude A can be derived using standard techniques by inserting the expansions for u and v into Eqs. (1). The result is the forced complex Ginzburg–Landau (FCGL) equation [33,34]:

$$A_t = (\mu + i\nu)A - (1 + i\beta)|A|^2 A + (1 + i\alpha)\nabla^2 A + \gamma\bar{A}, \quad (2)$$

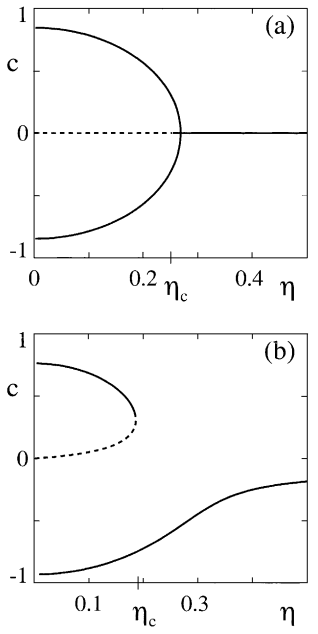

Fig. 1. The NIB bifurcation in the FHN model. The front speed, c, is shown as a solid curve for stable fronts and a dashed curve for unstable fronts. (a) The symmetric case, $a_0 = 0$ and (b) the nonsymmetric case, $a_0 \neq 0$.

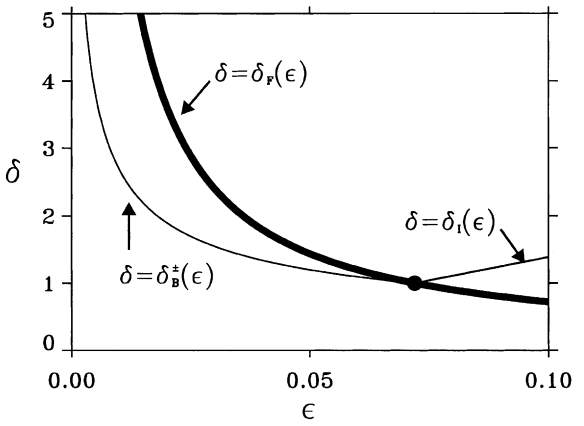

Fig. 2. The NIB bifurcation and planar-front transverse instability boundaries in the ϵ–δ parameter plane for a symmetric and isotropic model. The thick curve is the NIB bifurcation, $\delta_F(\epsilon) = \eta_c^2/\epsilon$. The thin curves are the boundaries for the transverse instability of Ising, $\delta_I(\epsilon)$, and Bloch, $\delta_B(\epsilon)$, fronts. When $\delta > \delta_I$ ($\delta > \delta_B$), planar Ising (Bloch) fronts are unstable to transverse perturbations. Parameters: $a_1 = 2.0$, $a_0 = 0$, $d = 0$.

where we rescaled the amplitude and the space and time coordinates, but for simplicity kept the same notation. In this equation, μ represents the distance from the Hopf bifurcation; ν represents the deviation of the system's oscillation frequency, $\frac{1}{2}\omega_f$, from the frequency, ω_0, of the unforced system; β represents a nonlinear correction of the oscillation frequency; α represents dispersion; and γ is the forcing strength. The forcing breaks the phase shift symmetry of Eq. (2), $A \to A\exp(i\phi)$, where ϕ is an arbitrary constant.

Eq. (2) has two stable constant solutions, A_0 and A_π with the properties, $|A_0| = |A_\pi|$ and $\arg A_\pi - \arg A_0 = \pi$. The two solutions describe uniform oscillations of the original system (1), with constant phases of oscillation, differing by π with respect to one another. In this respect, the forced oscillatory system is actually a bistable system and front solutions form that connect the two phase states in space. These front solutions undergo a NIB bifurcation similar to that found in the bistable FHN model. The bifurcation parameter is the forcing strength, γ. For γ larger than a critical value, γ_c, a single stable Ising front solution exists. The front is stationary and forms a fixed interface between the two phase states. As γ is decreased below γ_c, the stationary Ising front solution loses stability and a pair of counter-propagating Bloch front solutions appear.

In the following sections, we focus on the bistable form of the FHN model (with diffusion anisotropy, $d \neq 0$). Many of the findings associated with the NIB bifurcation are expected to hold for the forced oscillatory case as well.

3. Velocity of curved fronts in the presence of anisotropy

We study the effects of diffusion anisotropy on the dynamics of fronts in two space dimensions by deriving velocity–curvature relations for nearly planar fronts. The derivation uses a singular perturbation approach and is valid for $\lambda := \sqrt{\epsilon/\delta} \ll 1$. Relations of this kind have proved invaluable for qualitative prediction of pattern formation processes in isotropic systems such as spot replication and spiral wave nucleation [11,12,35–37].

We first transform to an orthogonal coordinate system (r, s) that moves with the front, where r is a coordinate normal to the front and s is the arclength. We denote the position vector of the front by $\mathbf{X}(s,t) = (X, Y)$, and define it to coincide with the $u = 0$ contour. The unit vectors tangent and normal to the front are given by

$$\hat{\mathbf{s}} = \cos\theta\,\hat{\mathbf{x}} + \sin\theta\,\hat{\mathbf{y}}, \qquad \hat{\mathbf{r}} = -\sin\theta\,\hat{\mathbf{x}} + \cos\theta\,\hat{\mathbf{y}},$$

where $\theta(s,t)$ is the angle that $\hat{s}$ makes with the x-axis. A point $\mathbf{x} = (x, y)$ in the laboratory frame can be expressed as

$$\mathbf{x} = \mathbf{X}(s,t) + r\hat{\mathbf{r}}.$$

This gives the following relation between the laboratory coordinates (x, y, t) and the coordinates (s, r, τ) in the moving frame:

$$\begin{aligned} x &= X(s,t) - r\sin\theta(s,\tau), \\ y &= Y(s,t) + r\cos\theta(s,\tau), \qquad t = \tau, \end{aligned} \tag{3}$$

where $\hat{\mathbf{s}} = \partial\mathbf{X}/\partial s$ and $\partial X/\partial s = \cos\theta$, $\partial Y/\partial s = \sin\theta$. In the moving frame coordinates, the front normal velocity and curvature are given by $C_n = -\partial r/\partial t$ and $\kappa = -\partial\theta/\partial s$, respectively.

The second step is to express Eqs. (1) in the moving frame and use singular perturbation theory, exploiting the smallness of λ. We distinguish between an inner region that includes the narrow front structure, and outer regions on both sides of the front. In the inner region $\partial u/\partial r \sim \mathcal{O}(\lambda^{-1})$ and $\partial v/\partial r \sim \mathcal{O}(1)$. In the outer regions both $\partial u/\partial r$ and $\partial v/\partial r$ are of order unity. In the inner region $v = v_f$ is taken to be constant. Expanding both u and v_f as powers series in λ and using these expansions in the moving frame equations we obtain at order unity

$$C_n = -\frac{3}{\eta\sqrt{2}} I(\theta) v_f - \frac{1+d}{\delta I(\theta)^2}\kappa, \tag{4}$$

where $I(\theta) = \sqrt{1 + d\cos^2\theta}$. In the outer regions to the left and to the right of the front region different approximations can be made. Here, $\partial u/\partial r \sim \partial v/\partial r \sim \mathcal{O}(1)$ and to leading order all terms containing the factor λ can be neglected. The resulting equations can be solved for v in the two outer regions. Continuity of v and of $\partial v/\partial r$ at the front position $r = 0$ yield a second relation between C_n and v_f. Eliminating v_f by inserting this relation into Eq. (4) gives an implicit relation between the normal velocity of the front and

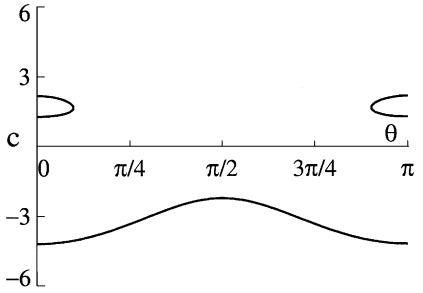

Fig. 3. The velocity of planar ($\kappa = 0$) fronts at different angles. Bloch fronts exist in narrow sectors around $\theta = 0$ and $\theta = \pi$. The wider sectors in between correspond to Ising fronts.

its curvature

$$C_{\mathrm{n}} + \frac{1+d}{\delta I(\theta)^2}\kappa = \frac{3I(\theta)(C_{\mathrm{n}}+\kappa)}{\eta\sqrt{2}q^2\sqrt{(C_{\mathrm{n}}+\kappa)^2+4q^2}} + \frac{3I(\theta)a_0}{\eta\sqrt{2}q^2}, \tag{5}$$

where $q^2 = a_1 + \frac{1}{2}$. More details about this derivation can be found in [26].

An example of the angular dependence of the velocity of a planar front, obtained by solving Eq. (5) at $\kappa = 0$ is shown in Fig. 3. The existence of a single front branch at $\theta = \pi/2$ implies an Ising front when the propagation is in the x direction, whereas the appearance of three front branches near $\theta = 0$ and $\theta = \pi$ implies coexistence of Bloch fronts when the propagation is in the y direction.

Typical velocity–curvature relations obtained as solutions of Eq. (5) for a given θ value are shown in Fig. 4. The number of intersection points with the $\kappa = 0$ axis indicates the number of planar front solutions. Positive slopes at these points indicate instability to transverse perturbations. Termination points of lower or upper branches close to the $\kappa = 0$ axis indicate proximity to the NIB bifurcation and a likelihood for spontaneous front transitions, i.e., dynamic transitions between the two branches leading to reversals in the direction of front propagation [12,35,37,38]. These transitions can be induced by curvature variations, as Fig. 4 suggests, as well as by other perturbations like front interactions. Relations between the front velocity and its distance to a nearby front or a boundary can be similarly derived [39].

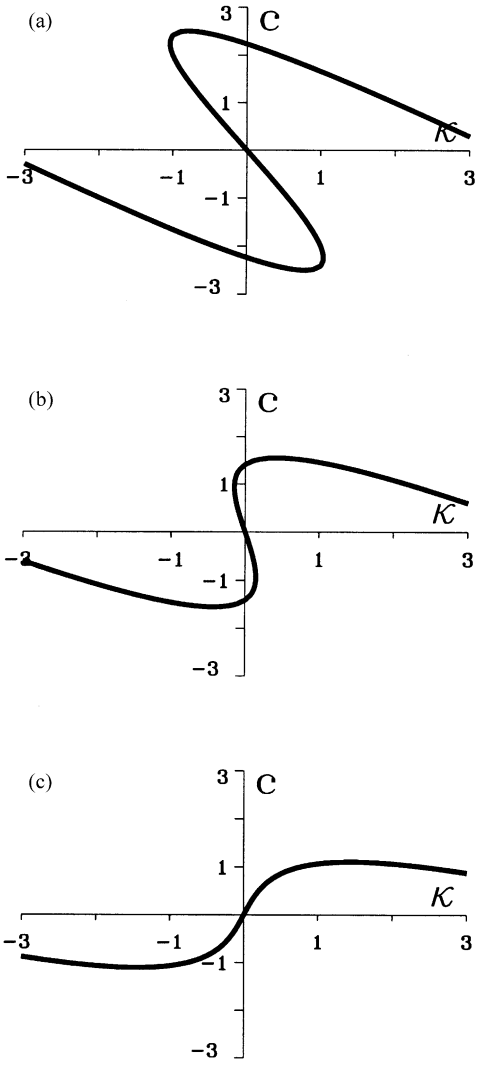

Fig. 4. Typical velocity–curvature relations of Eq. (5). (a) In the "Bloch regime" where both planar front solutions exist and are stable to transverse perturbations, $\delta = 1.2$. (b) Near the front bifurcation where two planar front solutions exist but are unstable to transverse perturbations. The solution branches terminate near small values of the curvature κ, $\delta = 1.5$. (c) In the "Ising regime" only a single (in this case transversely unstable) planar front exists, $\delta = 2.5$. Other parameters: $a_1 = 2.0$, $a_0 = 0.0$, $\epsilon = 0.04$.

4. Stability of planar fronts

Eq. (5) can be used to study the effects of anisotropy on the stability properties of planar fronts. We begin with the NIB bifurcation. Consider the symmetric

model with $a_0 = 0$. Setting $\kappa = 0$, we find the Ising front solution $C_0 = 0$ and the two Bloch front solutions

$$C_0 = \pm\frac{2q}{\eta}\sqrt{\eta_c^2 I^2(\theta) - \eta^2}, \tag{6}$$

for $\eta < \eta_c I(\theta)$, where η_c is the NIB bifurcation point for the isotropic system and we recall that $\eta = \sqrt{\epsilon\delta}$. We have used the notation C_0 for the velocity of a planar front. The anisotropy shifts the bifurcation point by the factor $1 \le I \le 1 + d$:

$$\eta_c^{\text{anis}}(\theta) = \eta_c I(\theta). \tag{7}$$

In the ϵ–δ plane the front bifurcation boundary is given by

$$\delta = \delta_F = \frac{9}{8q^6}\frac{I^2(\theta)}{\epsilon}. \tag{8}$$

The stability of the Ising and Bloch fronts to transverse perturbations can be studied by linearizing Eq. (5) around $\kappa = 0$. This yields relations of the form

$$C_n = C_0 - D\kappa, \tag{9}$$

where C_0 is one of the three front solutions (an Ising front and a pair of Bloch fronts). The condition $D = 0$ gives the transverse instability threshold of the planar front solutions. For the symmetric system ($a_0 = 0$) we obtain

$$\delta = \delta_I = \frac{8q^6}{9}\frac{(1+d)^2\epsilon}{I^6(\theta)} \tag{10}$$

for the Ising front, and

$$\delta = \delta_B = \frac{3}{2\sqrt{2}q^3}\frac{\sqrt{1+d}}{\sqrt{\epsilon}} \tag{11}$$

for the Bloch fronts. Notice that the transverse instability threshold for Bloch fronts (in the symmetric case) is independent of the angle θ. Fig. 5 shows the NIB bifurcation boundary and the transverse instability boundaries for $\theta = 0$ (solid curves) and for $\theta = \pi/2$ (dashed curves) assuming a symmetric system, $a_0 = 0$.

In the nonsymmetric case ($a_0 \neq 0$), it is still possible to find an analytical expression for the threshold of the NIB bifurcation, $\eta_c^{\text{anis}}(\theta)$. This threshold occurs when the $\kappa = 0$ curve is tangent to the cubic C_n–κ curve that solves Eq. (5). We first solve for the value of C_n at this point by deriving Eq. (5) with respect to C_n and setting $d\kappa/dC_n = \kappa = 0$. Using this value of C_n in Eq. (5) with $\kappa = 0$ gives the threshold

$$\eta_c^{\text{anis}}(\theta) = \eta_c I(\theta)(1 - a_0^{2/3})^{3/2}. \tag{12}$$

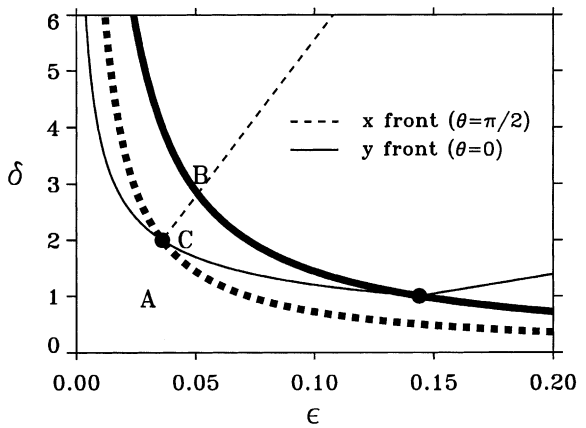

Fig. 5. The NIB bifurcation and planar-front transverse instability boundaries in the ϵ–δ parameter plane for the symmetric ($a_0 = 0$) and anisotropic ($d \neq 0$) case. The dashed curves are for the case of planar fronts propagating in the x direction ($\theta = \pi/2$) and the solid curves are for planar fronts propagating in the y direction ($\theta = 0$). The thick curves are the front bifurcation and the thin curves are the transverse instability boundaries of Ising and Bloch fronts. Note that the transverse instability boundaries for Bloch fronts in the x and y directions coincide. Parameters: $a_1 = 2$, $a_0 = 0$, $d = 1$.

Fig. 5 shows three points labeled A, B, C at parameter values where different spatiotemporal dynamics are expected to be found. At A, there are stable Bloch fronts in both the x and y directions. The Bloch fronts in the y direction are faster because the distance of the point A to the solid NIB bifurcation boundary is larger than the distance to the dashed NIB bifurcation boundary (see Fig. 1(a) for the dependence of Bloch front velocity on the distance to the NIB bifurcation point). At B, there are Ising fronts in both the x and y directions that are unstable to transverse perturbations. At C, there are stable Ising fronts in the x direction and unstable Bloch fronts in the y direction. In the nonsymmetric case ($a_0 \neq 0$), there are additional possibilities since the two Bloch fronts are no longer symmetric and their transverse instability boundaries are not degenerate [26]. In Section 5, we consider three pattern

formation mechanisms in conditions closely related to the points A, B, C, but in a nonsymmetric system.

5. Pattern formation mechanisms

Anisotropy may introduce mechanisms for pattern formation that do not exist in isotropic system. We present three examples. The first simply shows a distortion of a wave pattern due to diffusion anisotropy. The distortion may be strong but does not change the nature of the pattern. The second demonstrates an ordering effect of anisotropy where a labyrinthine pattern transforms into an ordered stripe pattern. The last demonstrates a confinement of spatiotemporal chaos to one space dimension.

Isotropic bistable systems in the Bloch regime produce traveling wave phenomena including rotating spiral waves. Fig. 6 shows the development of an oval spiral wave from a front line, consisting of two Bloch fronts, in the presence of anisotropy. The diffusion anisotropy causes the Bloch fronts propagating in the y direction to move faster than those propagating in the x direction as the velocity–curvature relations depicted in Fig. 7 show. Note the negative slopes of the Bloch front branches which imply stability to transverse perturbations. In the Ising regime, isotropic bistable systems may form stationary labyrinthine patterns as shown in Fig. 8(a). The pattern was obtained by numerical solution of Eqs. (1) with $d = 0$. Switching on anisotropic diffusion ($d \neq 0$) but keeping both the x and the y directions in the Ising regime leads to an ordering process where the pattern approaches regular stripes oriented parallel to the y direction as shown in Figs. 8(b)–(d). The selection of the y direction follows from the stronger transverse instability of planar and weakly curved fronts in this direction

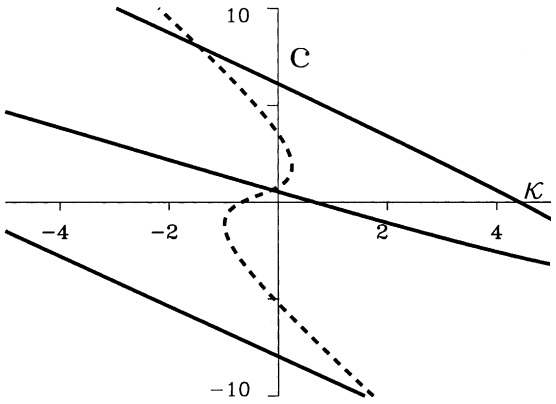

Fig. 7. Velocity vs curvature relation for Fig. 6. The solid (dashed) curves pertain to fronts propagating in the y (x) direction. Parameters: $a_1 = 2.0$, $a_0 = -0.1$, $\epsilon = 0.03$, $\delta = 0.8$, $d = 1$.

as indicated by the velocity–curvature relation shown in Fig. 9. Notice that the weaker transverse instability of fronts propagating in the x direction is suppressed due to front interactions. Similar behavior is expected when the difference in transverse instability strengths is greater or when a front propagating in the x direction is transversally stable.

In the two examples discussed above, the front type (Ising or Bloch) did not switch as the direction of propagation changed from x to y. Fig. 10 shows an example of velocity–curvature relations where Bloch fronts propagating in the y direction become stable Ising fronts when the propagation direction changes to x. Fig. 11 shows a numerical solution of Eqs. (1) starting with an isotropic disordered state. As time evolves, strong irregular dynamics become confined to the y direction and a state we term *stratified chaos* develops. Segments oriented in the y direction grow at their tips and either merge into larger segments or emit traveling

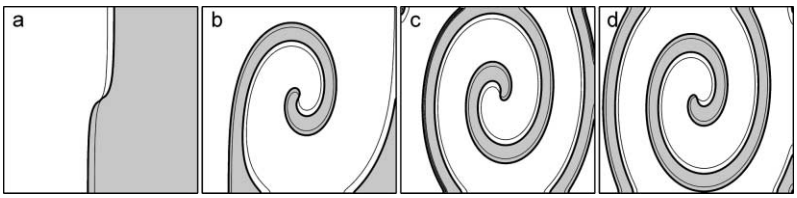

Fig. 6. Formation of an anisotropic spiral wave of Eqs. (1) with parameters corresponding to stable Bloch fronts in both the x and y directions. The shaded regions are up-state domains. Thick (thin) curves are $u = 0$ ($v = 0$) contours. The $v = 0$ line always lags behind the $u = 0$ line. Parameters: $a_1 = 2.0$, $a_0 = -0.1$, $\epsilon = 0.03$, $\delta = 0.8$, $d = 1$.

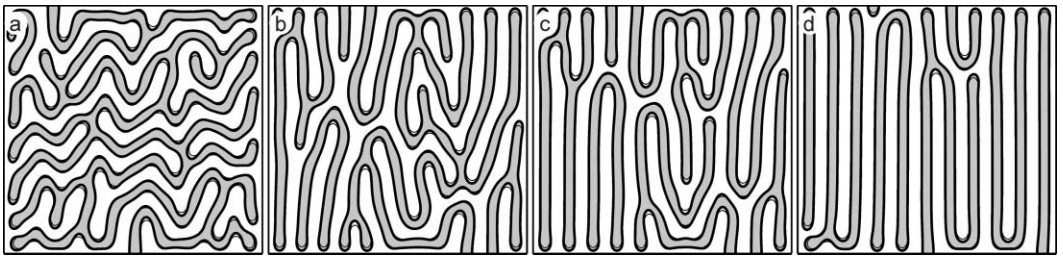

Fig. 8. Ordering effect in the Ising regime. An initial labyrinthine pattern evolves towards an ordered stripe pattern. Fronts propagating in the x and y directions are both unstable to transverse perturbations but the instability is stronger in the y direction. Parameters: $a_1 = 2.0$, $a_0 = -0.1$, $\epsilon = 0.03$, $\delta = 4.0$, $d = 1$.

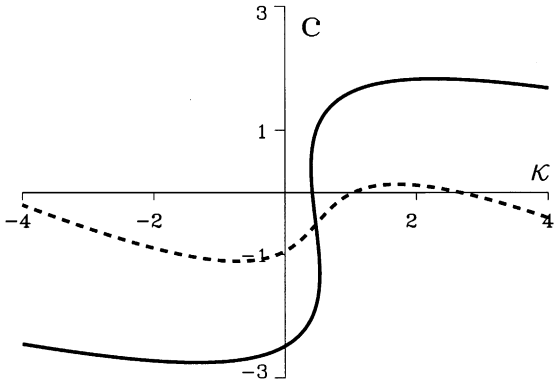

Fig. 9. Velocity vs curvature relation for Fig. 8. The solid (dashed) curves pertain to fronts propagating in the y (x) direction. Parameters: $a_1 = 2.0$, $a_0 = -0.1$, $\epsilon = 0.03$, $\delta = 4.0$, $d = 1$.

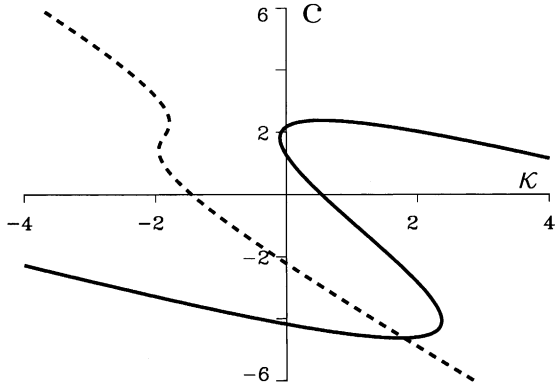

Fig. 10. Velocity vs curvature relation for Fig. 11. The solid (dashed) curves pertain to fronts propagating in the y (x) direction. Parameters: $a_1 = 2.0$, $a_0 = -0.1$, $\epsilon = 0.039$, $\delta = 1.7$, $d = 1$.

segments which grow new tips. In the x direction, a nearly regular periodic structure is maintained.

To quantify the irregular character of the dynamics in the y direction and the regular dynamics in the x direction, we computed the normalized spatial two-point correlation functions, $C_y(r)$ and $C_x(r)$, for the u field in both the x and the y directions. These correlation functions are given by

$$C_y(r) = \frac{\langle \Delta u(x, y + r) \Delta u(x, y) \rangle}{\langle \Delta u(x, y)^2 \rangle},$$

$$C_x(r) = \frac{\langle \Delta u(x + r, y) \Delta u(x, y) \rangle}{\langle \Delta u(x, y)^2 \rangle},$$

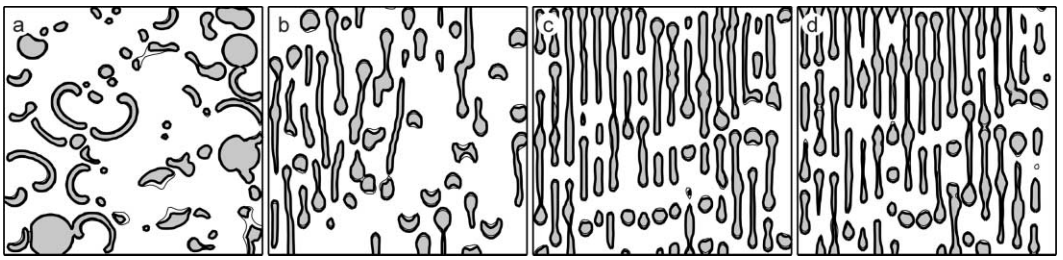

Fig. 11. Development of stratified chaos in Eqs. (1) with parameters corresponding to an Ising front in the x direction and to Bloch fronts in the y direction. Parameters: $a_1 = 2.0$, $a_0 = -0.1$, $\epsilon = 0.039$, $\delta = 1.7$, $d = 1$.

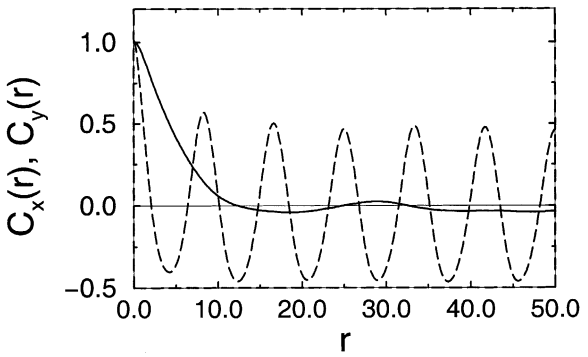

Fig. 12. Correlation functions $C_x(r)$ (dashed curve) and $C_y(r)$ (solid curve) for a state of stratified chaos.

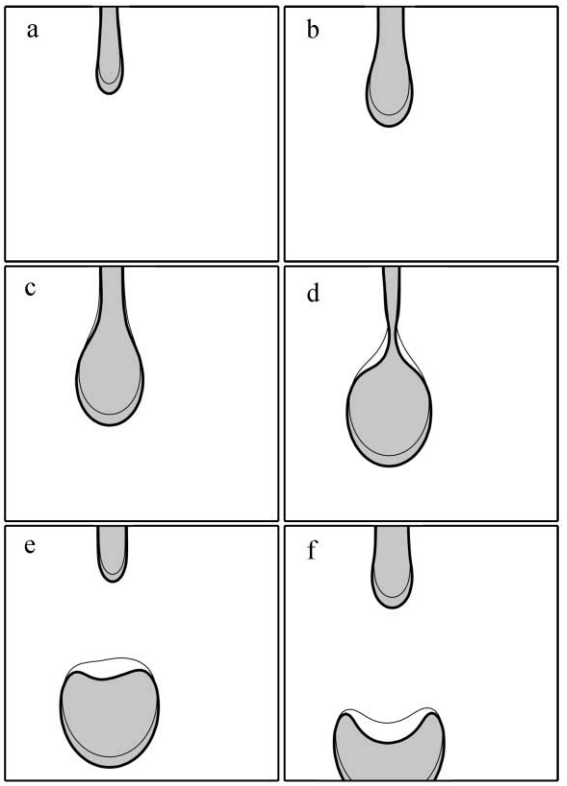

Fig. 13. Close-up of repeated segment formation. Shaded regions are up-state domains. Thick (thin) curves are $u = 0$ ($v = 0$) contours. The $v = 0$ contour always lags behind the $u = 0$ contour. The tip of a stripe segment (a) grows outward (b)–(c). A pinching dynamic begins (d) which leads to segment formation (e) traveling along the y direction (f). The segment formation leaves a shortened stripe segment (e) whose tip grows outward again (f) and the process repeats. The parameters are the same as in Fig. 10.

where $\Delta u(x, y) = u(x, y) - \langle u \rangle$, and the brackets $\langle\,\rangle$ denote space and time averaging. Fig. 12 shows the results of these computations. Correlations in the y direction decay to 0 on a length scale much smaller than the system size which is a characteristic of spatiotemporal chaotic systems. In contrast, correlations in the x direction oscillate with constant amplitude. This observation may be used to define stratified chaos as a state that displays finite correlation length in one direction (x) and infinite correlation length in the other (y).

A typical segment formation, occurring in the y direction, is illustrated in Fig. 13. The mechanism for this process relies strongly on the transition from an Ising front in the x direction to a Bloch front in the y direction. In the x direction, a pair of fronts approaching one another ("white" invading "gray" fronts in Fig. 13) repel and form stationary or breathing stripes. In the y direction, a pair of approaching fronts collapse and the domains following them merge. Imagine a segment tip growing into a bulge as in Fig. 13(a)–(c). At the neck of the bulge, propagation directions deviating from the x-axis develop and front collapse may occur. This leads to the detachment of a traveling segment as shown in Fig. 13(d)–(f).

6. Conclusion

The coupling of diffusion anisotropy to front instabilities in bistable systems may lead to new pattern formation mechanisms. A system with a single stable front in the x direction (stable Ising front) and a single unstable front in the y direction (unstable Ising front) tends to develop periodic stripe patterns aligned along the y direction. A system with a single stable (Ising) front in the x direction and a pair of counter-propagating (Bloch) fronts in the y direction may develop "stratified chaos", a state characterized by irregular dynamics confined to one space dimension. Additional new mechanisms of pattern formation are likely to be found by exploring different combinations of front stability and multiplicity in two orthogonal directions.

We studied the FHN type model but similar mechanisms are expected to be found in the FCGL equation (2) which describes periodically forced oscillatory systems. We only considered diffusion anisotropy but other forms of anisotropy are likely to have similar effects as they may also produce different front proper-

ties (stability, dynamics and multiplicity) in orthogonal directions. These expectations should be tested using realistic models of catalytic surface reactions, e.g., the NO + CO reaction on Pt(1 0 0) [40], the $O_2 + H_2$ [41], and the NO + H_2 [42] reactions on Rh(1 1 0).

Acknowledgements

This research was supported by a grant from the GIF, the German–Israeli Foundation for Scientific Research and Development. AH is supported by the Department of Energy under contract W-7405-ENG-36.

References

[1] R. Imbihl, G. Ertl, Chem. Rev. 95 (1995) 697.
[2] H.H. Rotermund, W. Engel, M. Kordesch, G. Ertl, Nature 343 (1990) 355.
[3] J. Lauterbach, H.H. Rotermund, Surf. Sci. 311 (1994) 231.
[4] H.H. Rotermund, S. Jakubith, A. von Oertzen, G. Ertl, Phys. Rev. Lett. 66 (1991) 3083.
[5] S. Jakubith, H.H. Rotermond, A. von Oertzen, G. Ertl, Phys. Rev. Lett. 65 (1990) 3013.
[6] G. Veser, F. Mertens, A. Mikhailov, R. Imbihl, Phys. Rev. Lett. 71 (1993) 935.
[7] R. Imbihl, A.E. Reynolds, D. Kaletta, Phys. Rev. Lett. 67 (1991) 725.
[8] M.I. Monine, L.M. Pismen, Catal. Today, same issue, Unpublished.
[9] L.M. Pismen, R. Imbihl, B.Y. Rubinstein, M. Monine, Phys. Rev. E 58 (1998) 2065.
[10] A. Hagberg, E. Meron, Nonlinearity 7 (1994) 805.
[11] A. Hagberg, E. Meron, Phys. Rev. Lett. 72 (1994) 2494.
[12] A. Hagberg, E. Meron, Chaos 4 (1994) 477.
[13] H.H. Rotermund, S. Jakubith, A. von Oertzen, G. Ertl, Phys. Rev. Lett. 65 (1990) 3013.
[14] G. Haas, et al., Phys. Rev. Lett. 75 (1995) 3560.
[15] P. Coullet, J. Lega, B. Houchmanzadeh, J. Lajzerowicz, Phys. Rev. Lett. 65 (1990) 1352.
[16] P. Coullet, K. Emilsson, Physica D 61 (1992) 119.
[17] M. Eiswirth, G. Ertl, Phys. Rev. Lett. 60 (1988) 1526.
[18] M. Bär, C. Zülicke, M. Eiswirth, G. Ertl, J. Chem. Phys. 96 (1992) 8595.
[19] M. Berdau, et al., J. Chem. Phys. 110 (1999) 11551.
[20] M. Bär, et al., Phys. Rev. Lett. 74 (1995) 1246.
[21] N. Gottschalk, et al., Phys. Rev. Lett. 73 (1994) 3483.
[22] M. Berdau, et al., J. Chem. Phys. 106 (1997) 4291.
[23] H. Ikeda, M. Mimura, Y. Nishiura, Nonlinear Anal.-Theor. Meth. Appl. 13 (1989) 507.
[24] M. Bode, A. Reuter, R. Schmeling, H.-G. Purwins, Phys. Lett. A 185 (1994) 70.
[25] M. Bär, A. Hagberg, E. Meron, U. Thiele, Phys. Rev. Lett. 83 (1999) 2664.
[26] M. Bär, A. Hagberg, E. Meron, U. Thiele, Phys. Rev. E 62 (2000) 366.
[27] F. Mertens, R. Imbihl, Nature 370 (1994) 124.
[28] A. Schaak, R. Imbihl, J. Chem. Phys. 107 (1997) 4741.
[29] A. Schaak, R. Imbihl, Chem. Phys. Lett. 283 (1998) 386.
[30] G. Flätgen, K. Krischer, J. Chem. Phys. 103 (1995) 5428.
[31] C. Elphick, A. Hagberg, E. Meron, B. Malomed, Phys. Lett. A 230 (1997) 33.
[32] D. Walgraef, Spatio-temporal Pattern Formation, Springer, New York, 1997.
[33] J.M. Gambaudo, J. Diff. Eq. 57 (1985) 172.
[34] C. Elphick, G. Iooss, E. Tirapegui, Phys. Lett. A 120 (1987) 459.
[35] C. Elphick, A. Hagberg, E. Meron, Phys. Rev. E 51 (1995) 3052.
[36] A. Hagberg, E. Meron, I. Rubinstein, B. Zaltzman, Phys. Rev. E 55 (1997) 4450.
[37] A. Hagberg, E. Meron, Physica D 123 (1998) 460.
[38] A. Hagberg, E. Meron, Phys. Rev. Lett. 78 (1997) 1166.
[39] D. Haim, et al., Phys. Rev. Lett. 77 (1996) 190.
[40] J. Christoph, et al., Phys. Rev. Lett. 82 (1999) 1586.
[41] A. Makeev, R. Imbihl, J. Chem. Phys. 113 (2000) 3854.
[42] A. Schaak, et al., Phys. Rev. Lett. 83 (1999) 1882.